Journal of Non-Crystalline Solids 505 (2019) 252–259

Contents lists available at ScienceDirect

Journal of Non-Crystalline Solids

journal homepage: www.elsevier.com/locate/jnoncrysol

Creation of glass-characteristic point defects in crystalline SiO_2 by 2.5 MeV electrons and by fast neutrons

Linards Skuja[a,*], Nadège Ollier[b], Koichi Kajihara[c], Krisjanis Smits[a]

[a] Institute of Solid State Physics, University of Latvia, 8 Kengaraga str, LV1063 Riga, Latvia
[b] Laboratoire des Solides Irradiés Ecole Polytechnique, University of Paris-Saclay, 91128 Palaiseau, France
[c] Department of Applied Chemistry for Environment, Graduate School of Urban Environmental Sciences, Tokyo Metropolitan University, 1-1 Minami-Osawa, Hachioji, Tokyo 192-0397, Japan

ARTICLE INFO

Keywords:
Silica glass
Quartz
Dangling bonds
Electron irradiation
Luminescence
Amorphization

ABSTRACT

Point defects in crystalline SiO_2, created by 2.5 MeV electron irradiation at dose below the amorphization threshold or by fast neutrons, were compared by luminescence spectroscopy. Oxygen dangling bonds ("non-bridging oxygen hole centers", NBOHCs), peculiar to amorphous state of SiO_2, were detected for the first time in electron-irradiated non-amorphized α-quartz crystal. Their presence may signal the formation of nucleation centers in crystal structure as the first step to radiation-induced amorphization. Compared to crystal, irradiated by 10^{19} cm^{-2} fast neutrons, their concentration was over 100 times lower, and their inhomogeneous broadening was at least 2.5 times smaller. Divalent silicons ("silicon oxygen deficiency centers", SiODC(II)), inherent to oxygen-deficient or irradiated SiO_2 glass, were detected in neutron-irradiated (10^{19} n/cm^2) α-quartz but were not found after the electron irradiation. Radiation-induced interstitial O_2 molecules, characteristic to irradiated glassy SiO_2 and other oxide glasses, are found in α-quartz only after neutron irradiation. The oxygen atoms, displaced by the 2.5 MeV e^- irradiation of α-quartz for fluences up to 10^{19} e^-/cm^2 evidently stays entirely in the peroxy linkage (Si-O-O-Si bond) form.

1. Introduction

Glassy SiO_2 ("silica", "quartz glass", "amorphous SiO_2") is the most important material for optical fiber waveguides, high-power laser optics and for radiation-resistant optics. Point defects in silica, created during the manufacturing or by irradiation are detrimental for most applications and have been treated in numerous works. As compared to single-crystal studies, spectroscopy of point defects in glass generally gives less information, due to their random orientation and much larger static site-to-site fluctuations ("inhomogeneous broadening") in glassy matrices. Therefore, for compounds, which exist both in crystalline and glassy states, it would be advantageous to use the crystal as a "test medium": to study the defects in detail in crystals, and then to apply the gained knowledge to the corresponding defects in glass.

Crystalline SiO_2 polymorph, α-quartz, is commonly considered as such "ordered counterpart" of glassy SiO_2. Both materials consist of corner-shared SiO_4 tetrahedra of nearly the same sizes. Si—O bond lengths are 160.4 and 161.3 pm in α-quartz [1] and ≈160 pm in silica [2]. The amorphous/glassy disorder is characterized by distributions of Si-O-Si angles, inter-tetrahedral torsional angles and medium-range connection topology (variations in the sizes of $(Si—O)_n$ (n = 3,4,5,6…) rings in the structure). These differences reduce the density of silica (2.20 g/cm^3) compared to α-quartz (2.65 g/cm^3). A frequently overlooked point is that they also radically change the nature of point defects in both materials. Indeed, the majority of the point defects present in amorphous SiO_2*are not* directly observable in crystalline SiO_2.

An exception from this rule is the simplest Frenkel defect, the oxygen vacancy, which is observed both in crystalline and glassy SiO_2 with nearly similar optical absorption (OA) bands at 7.6 eV [3]. In contrast, the dangling bond type defects, characteristic to glassy SiO_2, are completely absent in γ-irradiated non-amorphized α-quartz [3–6] and thus cannot be studied in a strictly crystalline environment. This is unfortunate, since these defects are the most important ones in optical applications of glassy SiO_2.

The oxygen dangling bond (siloxy radical, "non-bridging oxygen hole center", NBOHC) is a paramagnetic defect, which commonly gives the main contribution to radiation-induced OA in high purity silicas in the visible and in the mid-UV to vacuum-UV ranges [7,8]. The OA spectrum of NBOHCs is broad and typically overlaps with OA of other defects, therefore, apart from electron paramagnetic resonance (EPR)

* Corresponding author.
E-mail address: skuja@latnet.lv (L. Skuja).

https://doi.org/10.1016/j.jnoncrysol.2018.11.014
Received 30 August 2018; Received in revised form 7 November 2018; Accepted 14 November 2018
Available online 24 November 2018
0022-3093/

[9], its most reliable spectral fingerprint is photoluminescence (PL) band at 1.9 eV with decay time $\tau \approx (10-20)$ μs, excited into 2.0 and 4.8 eV OA bands, and showing zero-phonon line (ZPL) and vibronic structures under site-selective excitation [10,11]. NBOHCs are present in any irradiated silica or on the surface of activated SiO_2 particles [12], unless interstitial H_2 molecules have been added into glass to improve radiation toughness by converting NBOHCS to Si-O-H groups [13]. In contrast, despite the high sensitivity of the PL techniques, NBOHC's are not detected in γ-irradiated α-quartz [5,6]. Calculations show [14] that NBOHC's on surfaces of crystalline SiO_2 should have similar properties to NBOHCs in bulk silica.

Another intrinsic dangling bond type defect, divalent silicon ("type II silicon oxygen-deficiency center", "SiODC(II)") gives rise to an UV absorption band at 5.04 eV ("B_2" band) in oxygen –deficient or irradiated glassy SiO_2. It is commonly the main culprit for lowering of the UV-transmission limit in infrared-transmitting "dry" (Si-OH-free) optical fiber waveguides [15]. It shows 2 characteristic PL bands at 2.6 eV (τ = 10.2 ms [4]) and 4.4 eV (τ = 4 ns [16]). Similar to the case of NBOHC, these bands are absent in the PL spectra of γ-irradiated α-quartz [5,6].

The third intrinsic defect, inherent exclusively to the glassy form of SiO_2, is interstitial O_2 molecule, formed by dimerization of radiation-displaced oxygen atoms. It is created by irradiation both in silica [3,4,9,17,18] and in many multicomponent oxide glasses [19,20]. Apart from nuclear particle [18,21] or ionizing [17,18,22] radiation, interstitial O_2 is efficiently created in glassy SiO_2 as well by fs laser irradiation [23]. In contrast to silica, the interstitial O_2 in α-quartz is undetectable after γ-irradiation [3]. However it is found in quartz after particle irradiation [18], or after focused e^- irradiation in electron microscope beyond the amorphization fluence [22].

In this way, these three defects, NBOHC, SiODC(II), and interstitial O_2 may be roughly considered as inherent exclusively to the non-crystalline/disordered state of SiO_2. However, the situation is more nuanced in the case of nuclear particle (neutrons, ions) irradiation of crystalline SiO_2, when densely spaced multiple defects and local amorphized regions surrounded by crystal lattice can form in particle tracks. Dangling oxygen bonds with "crystal-like" properties: an ordered orientation, a small inhomogeneous broadening – were found in neutron-irradiated ("n-irradiated") quartz, evidently, on the boundaries between the crystalline and disordered regions. This was shown by site-selective PL and EPR study of NBOHC in n-irradiated quartz [24], using the intense and sharp zero-phonon lines of NBOHC at low temperatures. For defects in crystals, ZPLs should have distinct "fixed" peak positions, determined only by the defect structure and thus insensitive to small changes of excitation photon energy. In contrast, in glassy SiO_2 the disorder gives rise to a *continuous* Gaussian-shaped distribution of ZPL energies. Their emission peak positions follow the resonance ("site selective") excitation energies within this distribution. Its halfwidth (fwhm) is ≈80 meV for NBOHCs in the bulk silica [10] and 40 to 60 meV for NBOHCs on the surface of SiO_2 nanoparticles [12]. A superposition of both "crystal" and "glass" cases occurs in n-irradiated α-quartz: both "crystal-characteristic" ZPLs with well-defined (fixed) peak energies (fwhm < 1 meV) and energy-distributed (fwhm = 20 meV), "glass-characteristic" ZPLs of NBOHC are found [24].

Hence the presence of the PL of O dangling bonds (NBOHCs) in quartz can serve as a sensitive probe for the onset of local amorphization, and the ratio between the numbers of crystal-like and glass-like NBOHCs can reflect the growth of the amorphized regions.

Compared to the fast-neutron or ion irradiation, MeV electron irradiation is "softer", since it does not create single-particle tracks and locally disordered regions. Amorphization of α-quartz under focused electron microscope beam occurs first at very high fluences of $\approx 3 \times 10^{20}$ (2.5 MeV e^-)/cm^2 [25], see [26] for a recent review. Irradiation fluences $\approx 10^{19}$ cm^{-2} are reachable on linear electron accelerators. In this way, the onset of amorphization and the creation of dangling bond type defects in α-quartz just below the amorphization threshold can be explored.

As discussed above, apart from NBOHCs, two additional intrinsic defects can be regarded as peculiar to the glassy state of SiO_2: two-fold coordinated silicon SiODC(II) [4] and interstitial O_2 molecule [18]. The purpose of the present study is to check for the onset of creation of these three "glass-characteristic" defects in crystalline SiO_2 by e^- irradiation at doses below the amorphization threshold. That includes: (1) search for creation and spectral properties of oxygen dangling bonds in α-quartz irradiated with 2.5 MeV electrons below amorphization threshold doses; (2) to check for the creation of SiODC(II) defects in α-quartz by particle or e^- irradiation; and (3) to check for the possible interstitial O_2 formation in electron-irradiated α-quartz.

2. Experimental

2.1. Samples and irradiation

High purity synthetic α-quartz samples (Asahi Glass/Tokyo Denpa) with typical metallic impurity concentrations (according to manufacturer, in cm^{-3}): 2×10^{15} Al, 2×10^{15} Li, 1×10^{15} Na, 5×10^{13} Fe, 4×10^{13} Ge, similar to ones used in the previous work [3], were studied. They were irradiated by 2.5 MeV electrons using SIRIUS Pelletron linear accelerator at Ecole Polytechnique, Palaiseau with fluences between 1.2×10^{18} and 3.0×10^{19} e^-/cm^2, electron flux 5.5×10^{13} $e^-/(cm^2\,s)$ (dose rate 51 MGy/h) and sample temperature 60 °C. The absorbed dose was calculated from the electron stopping power tables for SiO_2 [27] to range from 0.30 to 7.62 GGy, respectively, with close to uniform energy deposition (within 90% for the thickest 0.5 cm sample). Electron-irradiated samples were compared to fast (E > 1 MeV) n-irradiated (1×10^{19} n/cm^2) and γ-irradiated (13 MGy) α-quartz samples, used in our previous work [18,24]. Three samples of synthetic SiO_2 glass were measured as a reference: (1) unirradiated oxygen deficient commercial KUVI type "dry" glass (< 5×10^{16} SiOH/cm^3; ≈10^{16} SiODC(II)/cm^3), (2) unirradiated oxygen-excess glass with 2.8×10^{17} interstitial O_2 molecules/cm^3 (type "Suprasil W"), and (3) n-irradiated (1×10^{19} n/cm^2) glass ("Suprasil W"), containing ≈1.1×10^{19} NBOHC/cm^3. The neutron- and γ-irradiations have been performed previously in "IRT-2000" research reactor. The fast neutron (E > 1 MeV) flux was 3×10^{13} $n/(cm^2\,s)$, energy distribution peak at 1.3 MeV, sample temperature ~200 °C. γ-irradiation was performed by liquid In-Ga-Sn alloy irradiation loop with ^{116}In as γ-ray source with average energy of 1.15 MeV and dose rate ~100 kGy/h, sample temperature ~80C. The native γ-ray background was not separated during the neutron-irradiations, since the radiation effects were dominated by neutrons.

2.2. Instrumentation

Time-resolved PL spectra were measured at the room temperature using 4th harmonic (266 nm, 4.66 eV) of Q-switched Nd-YAG laser (Quanta Ray Indi), pulse length 10 ns, energy 1.5 mJ. PL was recorded by a 193 mm focal length spectrograph (Andor Shamrock193i) equipped with iStar734–18 image-intensified CCD camera. Time-resolution better than 10 ns was facilitated by gating the image intensifier with a pulse of appropriate width, delayed relative to the laser pulse. Luminescence decay kinetics was obtained from series of spectra, taken by stepping the delay of a fixed-width time gate. The kinetics of the triplet luminescence of SiODC (II) centers in SiO_2 glass was measured using 250 nm excitation by mechanically chopped light of Xe-lamp, filtered through AMKO LTI 200 mm monochromator, with PL emission detected by Hamamatsu R955 photomultiplier and FastComtec 7882 multichannel counter.

CW-mode visible-to-UV range PL spectra were taken at temperatures between 14 K and 300 K with sample placed in closed-cycle He refrigerator (Leyboldt Heraeus RDK 10–320). The PL was recorded by 300 mm Andor Shamrock 303i spectrograph with Andor DU971N-UVB

cooled CCD camera. The excitation sources were CW He—Ne laser (5 mW, λ = 632.81 nm Thorlabs HNL050L) with Semrock LP01-633RS long-pass filter blocking the laser light, and 150 W Xe lamp, filtered through two (tandem) AMKO LTI 200 mm monochromators. The spectral resolution for low-T measurements with He—Ne laser excitation was 0.5 or 0.8 meV (full width at half maximum, fwhm determined using Ne spectral line at λ = 650.65 nm). The spectral calibration of Shamrock 303i spectrograph was finely adjusted at each used diffraction grating position by measuring the line-spectrum of Ne discharge lamp. This allowed for an accurate comparison between spectral positions of PL lines, obtained in different measurement sessions.

Near-infrared PL spectra of interstitial O_2 molecules were recorded at room temperature under 766 nm CW excitation by diode laser (700 mW, Leading Tech Laser Co, model ADR 1805), using AMKO LTI 200 mm monochromator and Hamamatsu R5509–43 liquid N_2-cooled photomultiplier tube. Spectral resolution was 5 nm (fwhm).

The Raman spectrum of the n-irradiated crystal was compared to that of pristine crystal using Fourier-transform infrared Raman spectrometer (Bruker Equinox, excitation at λ = 1064 nm, resolution 8 cm^{-1}).

3. Results

Since the red PL of oxygen dangling bonds (NBOHC) in SiO_2 glass has lifetime in 10…20 μs range, and an excitation band around 4.8 eV [10], time-resolved PL spectra in μs range with 4.66 eV excitation were measured (Fig. 1). The top trace (a) shows PL spectrum of electron-irradiated (7.62 GGy, 3×10^{19} cm^{-2}) α-quartz. Its peak position (1.90 eV) and fwhm (0.19 eV) is very close to their values for similar time-resolved PL peaks of n-irradiated α-quartz (1.89 eV, 0.17 eV, Fig. 1b) and of n-irradiated SiO_2 glass (1.90 eV, 0.17 eV, Fig. 1c). After correction for slightly different delay/gate parameters, it can be estimated that PL intensity of e^--irradiated crystal (Fig. 1a) is > 100 times lower than in the case of n-irradiated crystal (Fig. 1b). The slightly larger fwhm of the PL band in e^- irradiated quartz could be due to an additional unresolved component in the 2 to 2.3 eV range. A PL band, similar to Fig. 1a, with ≈100 times less intensity was observed as well in less-irradiated (1.2×10^{18} e^-/cm^2) quartz (not shown). No such PL band could be detected in time-resolved PL spectra of γ-irradiated (13

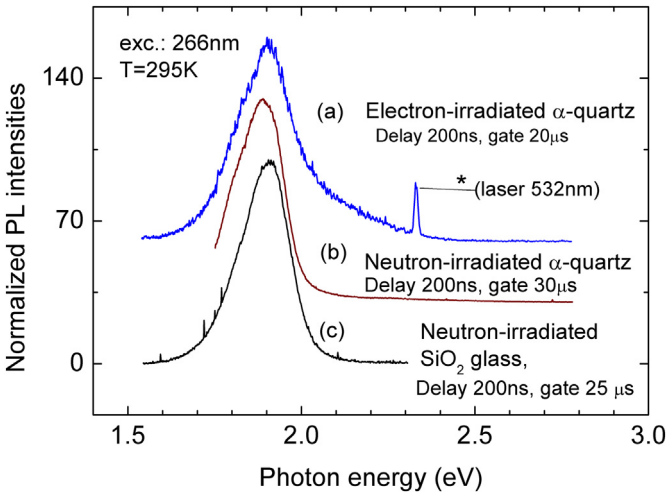

Fig. 1. Microsecond-range time-resolved photoluminescence spectra of 2.5 MeV electron-irradiated (3×10^{19} e^-/cm^2) α-quartz crystal (a), neutron-irradiated (1×10^{19} n/cm^2) α-quartz crystal (b), and neutron-irradiated (1×10^{19} n/cm^2) synthetic SiO_2 glass (c). Excitation energy was 4.66 eV (266 nm), the time-resolved luminescence was recorded during the time gate, delayed relative to the 10 ns laser pulse. Gate widths and delays are indicated at each spectrum. T = 295 K. The peak intensities are independently normalized, the spectra (a) and (b) are up-shifted by 30 and 60 arb. units for visibility.

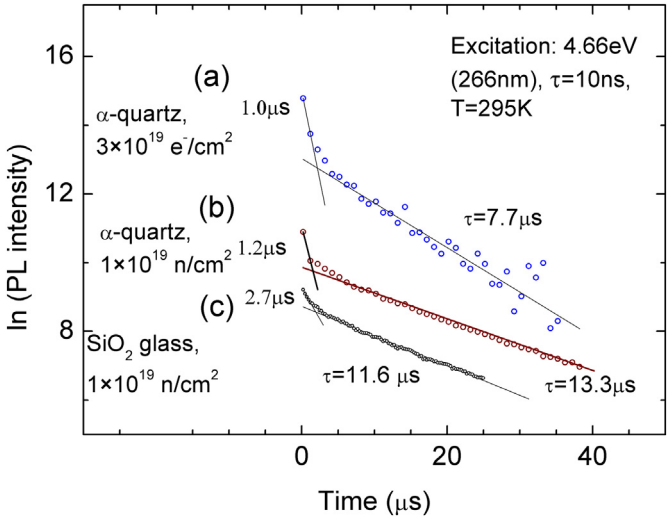

Fig. 2. Decay kinetics of the red photoluminescence in electron-irradiated α-quartz (a), neutron-irradiated α-quartz (b), and neutron-irradiated synthetic SiO_2 glass (c). Kinetics is obtained by integrating spectral regions (1.7–2.1) eV, (1.80–1.95) eV and (1.85–1.95) eV, respectively, which correspond to the peaks in luminescence spectra of Fig. 1.

MGy) or unirradiated α-quartz, measured under the same conditions. Its absence allows to estimate that it is over 2000 times weaker than the PL band in Fig. 1a.

The decay kinetics of the 1.9 eV PL bands of Fig. 1 are shown in Fig. 2. The solid lines show the linear least squares fits to PL kinetics drawn in semi-log scale. The common features for all three samples are a short component in 1 to 3 μs range and a longer component in 7 to 13 μs range. The decay of the 1.9 eV PL in the e^- −irradiated crystal is ≈2× shorter than that in n-irradiated glass. A comparison between the time-resolved spectra, measured during the first 3 μs and those measured at longer delay times (not shown), indicates that the short kinetics component is at least partially due to an admixture of an additional PL band in the 2 to 2.3 eV region.

Fig. 3 shows a comparison between the PL spectra of neutron- (top, panel (a)) and e^- −irradiated (bottom, panel (b)) α-quartz measured at temperatures between 14.5 K and 300 K with narrow-band (632.81 nm, 1.959 eV) excitation by He—Ne laser. Its energy falls into the region where sharp absorption lines of NBOHC are present [10] and therefore this excitation may be site-selective. Due to the much weaker PL intensity, the e^- −irradiated sample was measured with worse spectral resolution (fwhm = 0.8 meV) as compared to the spectra of n-irradiated sample (fwhm = 0.5 meV). Both sets of PL spectra show a number of sharp bands, marked by vertical lines, arbitrary enumerated towards descending energies. The solid lines indicate bands, present both in neutron- and e^- − irradiated samples, the dotted lines (#1, #3, #6) show bands observed only in one sample.

The peak positions and their “as measured” fwhm's are summarized in Table 1. The fwhm of some PL bands, (e.g., the line #2 at 1.928 eV, fwhm = 0.88 meV) in e^- -irradiated sample, are close to instrument resolution, (fwhm ≈ 0.8 meV@ 1.9 eV), indicating that the true half-widths of these lines are much smaller. However, the same line (#2) in n-irradiated quartz (Fig. 3, a) is measurably broader (fwhm = 1.99 meV, measured with resolution 0.5 meV) (Table 1). This allows to conclude that the true fwhm of this line in n-irradiated crystal is at least ≈ (5–10) times larger than in e^- −irradiated crystal.

Most of the sharp lines in spectra of Fig. 3 vanish on warming of the samples to 200 K. However, few lines (denoted as V1…V4) persist at the room temperature, indicating that they are most likely Raman lines of α-quartz. Indeed, their spectral shifts relative to the excitation wavelength (632.81 nm) are 207, 266, 357, and 466 cm^{-1} for lines V1, V2, V3, and V4, respectively. They correspond well to the reported Raman

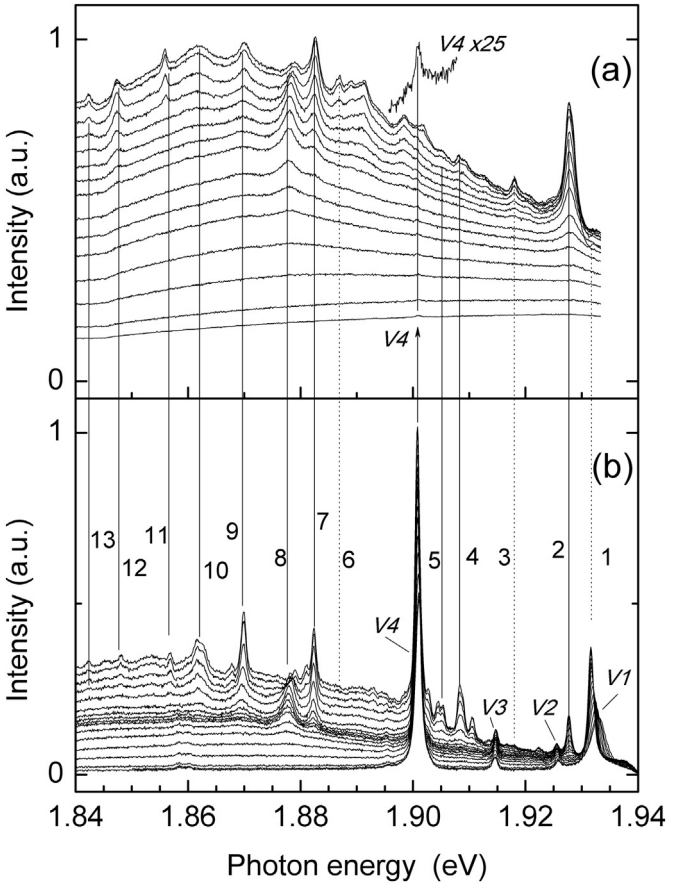

Fig. 3. Site-selective PL spectra of α-quartz irradiated by 1×10^{19} n/cm^2 (top panel (a)) and by 1.43×10^{19} e$^-$/cm^2 (bottom panel (b)). Excitation wavelength is 632.8 nm (1.959 eV). The measurement temperatures (in K) are (top-down): panel (a): 14.5, 20, 30, …, 70, 80, 100, 120, 140, 170, 200, 240, 270; panel (b): 14.5, 20, 30, …, 90, 100, 120, 140, 170, 200, 240, 270, 300 (K). Vibrational Raman lines V1…V4 correspond to Raman shifts 208, 264, 357, 466 cm^{-1}, respectively. Arrow at V4 (panel a, bottom trace) points to the low-intensity 466 cm^{-1} Raman band measured at $T = 270$ K. This band is shown in ×25 magnification (shifted) at the top. Vertical solid lines indicate PL peaks, detected in both samples, dotted lines (#1, #3, #6) point to PL peaks, resolved only in one sample. Both sets of spectra are independently normalized to 1 at $T = 14.5$ K and have a common baseline at 0. Spectral resolutions are 0.5 meV (a) and 0.8 meV (b).

line positions in α-quartz: 207 (A_1), 265 (E), 356 (A_1), and 464 (A_1) cm^{-1} [28]. The 207 cm^{-1} line shifts to 218 cm^{-1} and its fwhm decreases from 24 to 8 cm^{-1} upon cooling from 300 K to 14 K.

The presence of Raman lines allows for a correct comparison between PL line intensities in different samples by normalizing the PL intensities to the accompanying Raman line intensity. For the PL line at 1.928 eV (line #2 in Fig. 3 and Table 1) the intensity ratios relative to the 466 cm^{-1} Raman line (V4) are 206 and 0.124 for the n-irradiated and e$^-$ -irradiated samples, respectively. Hence the intensity of this PL line in n-irradiated sample is ≈1600 times stronger compared to that in the e$^-$ -irradiated sample.

The Raman spectrum of n-irradiated α-quartz in Fig. 3a is largely obscured by PL. The infrared Raman ($\lambda_{excit.} = 1064$ nm) spectrum of this sample (not shown) was free of PL background. It revealed no change in line positions or halfwidths as compared to pristine α-quartz. The fwhm of the dominant 466 cm^{-1} line was 17 cm^{-1} in both cases (spectrometer resolution 8 cm^{-1}). The position of 207 cm^{-1} line, which is known [29] to broaden and shift to 162 cm^{-1} upon quartz α-β phase transition, was not changed by n-irradiation.

Fig. 4 shows a comparison between the millisecond-range time-resolved PL spectra of n-irradiated and e$^-$ −irradiated α-quartz. The line marked by * is laser harmonic. Only the red PL band at 1.90 eV, similar to the one found in microsecond range (Fig. 1a) is observed for e$^-$ −irradiated crystal (Fig. 4, b). In contrast, in n-irradiated crystal an additional, “slow” PL band, which does not disappear after 300 μs delay after the laser pulse is observed with peak at 2.57 eV and fwhm 0.38 eV (Fig. 4, a). The decay kinetics of this band is exponential with $\tau = 8.7$ ms at $T = 295$ K (Fig. 5, top).

For comparison, the decay kinetics of the blue 2.7 eV triplet PL of SiODC(II) centers in oxygen deficient glassy SiO_2 is shown at the bottom, it yields an exponential decay constant $\tau = 9.9$ ms at T = 295 K.

Fig. 6. (Color online).Ultraviolet photoluminescence of neutron-

Table 1
Peak positions and their halfwidths (fwhm) in PL/Raman spectra of e$^-$-irradiated and neutron-irradiated α-quartz, measured at 14 K (Fig. 3). Spectrometer resolution was 0.8 meV and 0.5 meV, respectively. The corresponding Raman shifts at $T = 300$ K and symmetries for Raman lines V1-V4 are given in parentheses.

Peak # in Fig. 3	1.4×10^{19} e$^-$/cm^2		1.0×10^{19} neutrons/cm^2	
	Pos. (eV)	fwhm (meV, res. 0.8 meV)	Pos. (eV)	fwhm (meV, res. 0.5 meV)
1	1.932	1.10		
2	1.928	0.88	1.928	1.99
3			1.918	0.97
4	1.908	1.24	1.908	0.95
5	1.905	1.61	1.905	1.10
6			1.887	0.96
7	1.882	0.80	1.883	1.38
8	1.879	0.89	1.879	1.80
9	1.870	0.96	1.870	1.96
10	1.862	2.40	1.861	3.80
11	1.857	0.81	1.856	0.71
12	1.848	0.66	1.847	1.40
13	1.842	0.78	1.842	0.82
V1(208 cm^{-1}, A_1)	1.933	2.75		
V2 (266 cm^{-1}, E)	1.926	1.07		
V3 (357 cm^{-1}, A_1)	1.914	1.00		
V4 (466 cm^{-1}, A_1)	1.901	1.40	1.901	0.95

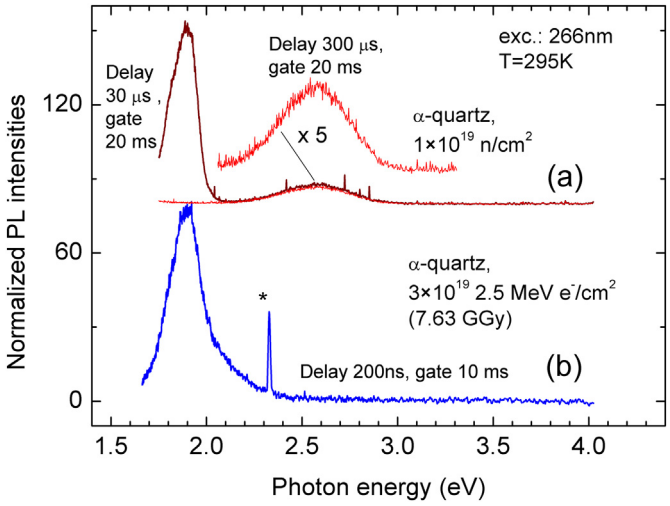

Fig. 4. Millisecond-range time-resolved photoluminescence spectra of α-quartz, irradiated by fast neutrons (1×10^{19} n/cm^2), (a) and by 2.5 MeV electrons (3×10^{19} e$^-$/cm^2) (b). Excitation by 4.66 eV (266 nm) 10 ns laser pulses, the PL was recorded during delayed time-gate. Gate widths and delays are indicated. The peak intensities are independently normalized, 30× higher gain was used for (b). Spectra (a) are up-shifted for visibility. The peak of the “slow band” in (a) is at 2.57 eV, halfwidth (fwhm) = 0.38 eV.

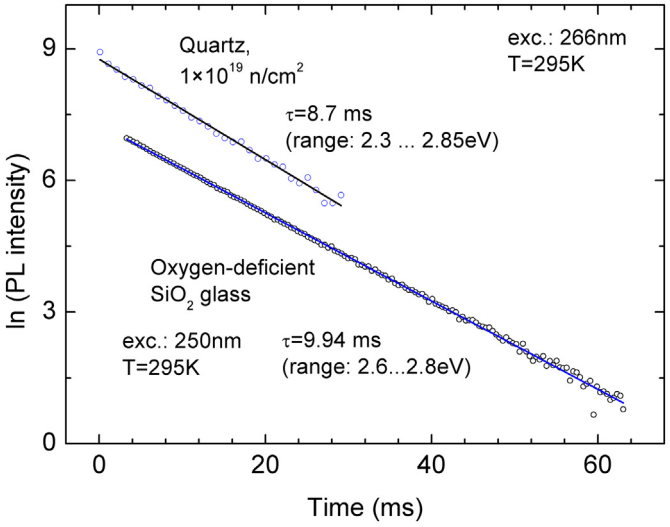

Fig. 5. Decay kinetics of the 2.6 eV luminescence band (Fig. 4) induced by neutron-irradiation of α-quartz (top) compared to the decay of the luminescence of the SiODC(II) – centers in unirradiated oxygen deficient SiO_2 glass (bottom).

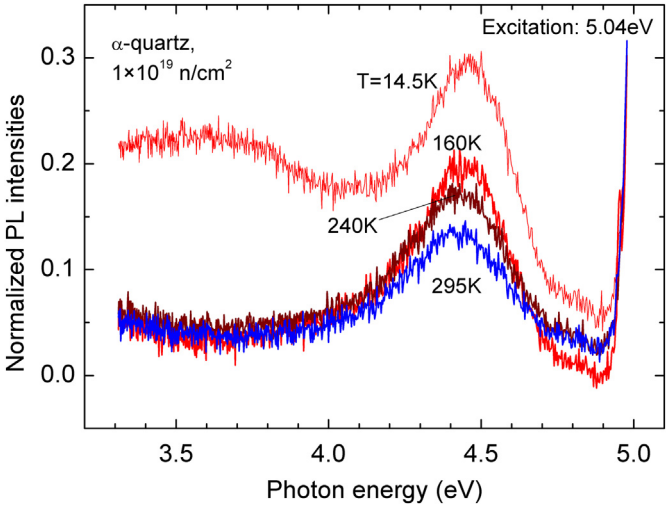

Fig. 6. Ultraviolet photoluminescence of neutron-irradiated (1×10^{19} n/cm^2) α-quartz under excitation at 5.04 eV, the peak position of the absorption band of SiODC(II) centers in SiO_2 glass. Spectral resolution 16 meV at 4.4 eV.

irradiated (1×10^{19} n/cm^2) α-quartz under excitation at 5.04 eV, the peak position of the absorption band of SiODC(II) centers in SiO_2 glass. Spectral resolution 16 meV at 4.4 eV.

The UV-range PL of n-irradiated crystal is shown in Fig. 6. A PL peak with peak at 4.38 eV and fwhm = 0.35 eV at T = 295 K is present under 5.04 eV excitation. On cooling to 14 K its intensity grows moderately and another PL peak at 3.5 eV appears (top curve). In e^- −irradiated sample the 4.38 eV PL band is completely absent, only the 3.5 eV PL band appears at low temperatures (spectrum not shown).

Fig. 7 shows the near-infrared PL spectra, recorded with 1.618 eV (766 nm) excitation at room temperature. The characteristic "singlet oxygen" PL band at ≈1283 nm (0.966 eV) due to interstitial O_2 molecules is present in n-irradiated quartz (trace b). It is completely absent in e^- −irradiated quartz samples (traces c,d). A sample of non-irradiated oxygen-rich SiO_2 glass containing 2.8×10^{17} O_2/cm^3 was measured as a reference (peak at 1275 nm, trace a).

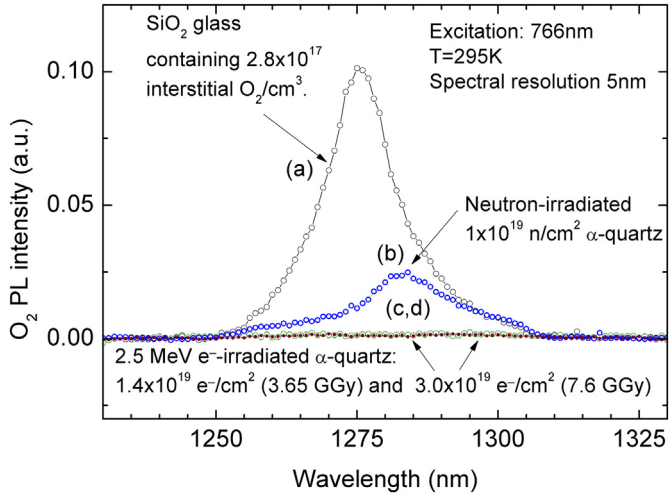

Fig. 7. Infrared luminescence of interstitial O_2 molecules in unirradiated SiO_2 glass, manufactured under oxygen-excess conditions (a) and of neutron irradiation-induced O_2 molecules in α-quartz (b). Luminescence of O_2 in electron-irradiated α-quartz was not detected (c,d). All spectra were taken under the same conditions.

4. Discussion

4.1. Oxygen dangling bonds

It is well-established (see [10,24] and references therein) that the ubiquitous 1.9 eV PL band in silica glass (Fig. 1c), which is also present in n-irradiated α-quartz (Fig. 1, b), is caused by oxygen dangling bonds (NBOHC). The peak position and fwhm of the PL spectrum of e^- −irradiated α-quartz (Fig. 1a) are similar to those of n-irradiated quartz or glass (Fig. 1a,b,c). Further, the lifetimes of the PL are very close in all three cases (Fig. 2). These similarities indicate that the red PL band in e^- irradiated quartz is due to NBOHCs. As far as we know, this is the first observation of NBOHCs in *non-amorphized* crystalline SiO_2, which has not been damaged by ion- or neutron-irradiation, capable of track formation. Additionally, the present data confirms the previously reported [5,6] absence of NBOHC PL in γ-irradiated quartz.

The assignment of the red PL in e^- −irradiated quartz is further supported by low-temperature site-selective PL spectra (Fig. 3). They show a number of sharp lines common both to n-irradiated (Fig. 3a) and e^- −irradiated (Fig. 3b) quartz. The line #7 at 1.882–1.883 eV has been previously identified as zero-phonon line [24] (named "ZPL2" in [30]) of a separate distinct sub-type of NBOHC's in n-irradiated quartz. The line #9 at 1.870 eV belongs to another sub-type of ordered NBOHC's. It coincides with the most intense line in the multiline structure ("L3" [30]) observed in time-resolved site-selective PL spectra of NBOHCs under near-resonance (1.879 eV) excitation.

The most intense line among the previously reported ZPLs of NBOHC in n-irradiated quartz is "ZPL1" at 1.933 eV [24,30]. However, it is absent in Fig. 3a, evidently because the energy of He—Ne laser photons (1.959 eV) does not exactly match the narrow near-resonance absorption/excitation lines of this sub-type of NBOHCs. In e^- −irradiated quartz (Fig. 3b) there is a 1.933 eV line at 300 K, which evidently is the 207 cm^{-1} Raman "soft mode" line of α-quartz [28]. It sharpens and shifts to 218 cm^{-1} (1.9316 eV absolute position) on cooling to 14 K. The strong T-dependence of this line and its sensitivity to quartz α-β transition is well-known [29].

The previous work [24] has shown that in n-irradiated quartz there are 2 groups of NBOHC's: (a) crystal-like, comprising several sub-types with distinct ZPL energies, (b) glass-like, embedded in disordered (amorphized) local environment and having much broader, continuous ZPL energy distribution. Comparison between Fig. 3a and b reveals that

the e^--irradiated sample has a higher sharp-line to broadband PL intensity ratio, as compared to n-irradiated quartz. Part of the broadband component is of homogeneous origin, due to the phonon sidebands, which should be similar for the same generic type of defect centers. The increased broadband intensity in the n-irradiated sample then indicates a larger inhomogeneous broadening, and/or a larger volume fraction of amorphized regions. The on- average higher crystalline order around NBOHC's sites in e^-- irradiated quartz is confirmed by the significantly smaller fwhm of the sharp PL lines in e^- − irradiated sample. For example, the fwhm of line #2 at 1.928 eV for e^- −irradiated sample is over 10 times narrower compared to it in n-irradiated sample (Results section and Table 1).

In this way, the "crystal-like" subset of NBOHCs in e^- − irradiated quartz exists in more ordered sites, as compared to n-irradiated quartz. Their concentration is, probably, quite low. The PL intensity at 295 K and UV excitation is > 100 times lower, compared to n-irradiated quartz (Fig. 1a,b). This ratio is even larger for the sharp features in low-T PL spectra, for example, it is ≈1600 for the intensities of the 1.928 eV line (#2, Fig. 3, T = 14 K). However, in the latter case the ratio can additionally depend on the exact energy of the excitation used (He—Ne laser, 1.959 eV in this case), since it can be accidentally selective, and has higher probability to be "off-resonance" with the narrower excitation/absorption lines in e^- −irradiated samples.

As signified by its name, the oxygen dangling bond has its terminal oxygen projecting into some structural void and interacting mainly only with its "own" SiO_4 tetrahedron, in approximate C_{3v} local symmetry ("basis interactions"). Interactions from the opposite side, ("void interactions") are much weaker. Luminescent NBOHCs are well-known to exist on SiO_2 surfaces [10,12,31]. The disorder around the surface NBOHC's, measured by the fwhm of the distribution of resonance ZPL energies was found to be smaller as compared to bulk NBOHCs (40 meV vs. 80 meV) [32]. The creation of NBOHCs in e^--irradiated quartz indicates a formation of internal voids of size comparable to voids in glassy SiO_2. The extreme sharpness of non-resonantly excited ZPLs in e^--irradiated quartz (Fig. 3) points to a creation of non-broadened NBOHC's, whose "basis interactions" are clearly with ordered crystalline SiO_2 lattice, while the "void interactions" are either negligible (large voids) or uniform, due to the same shape of all voids, causing all centers to be equal.

The average diameter of interstitial voids in silica glass is estimated as ≈5 Å from positron annihilation studies [33]. Similar size voids develop in α-quartz on n-irradiation of fluences > 10^{19} n/cm^2 [34] or after ion implantation [35]. In the case of e^- − irradiation of α-quartz it has been observed that disordered ("metamict") inclusions (diameter ≈10 nm at dose 10 GGy) initially grow heterogeneously, at irregularities of the crystal structure, most likely at precursor sites: hydroxyl impurities or dislocations [36]. The amorphization proceeds when sufficient concentration of point defects has accumulated and is complete at ≈ 1 TGy [36,37]. 2.2 MeV TEM study suggests even a lower amorphization dose of ≈100 GGy [25]. The present data (max. dose 7.62 GGy) do not allow to distinguish between the initial creation of voids at intact (intrinsic) quartz sites or from precursor-related sites. Calculations of NBOHCs on surfaces of different SiO_2 polymorphs have shown that their properties are only little changed by a presence of neighboring O—H group [14,38]. In the light of the previous works ([25,36,37]), the initial growth at precursor-sites is more likely.

4.2. Divalent Si - ODC(II)

Given the creation of "amorphous-state" defects (NBOHC's) in high-dose e^--irradiated quartz, it is of interest to look for a simultaneous creation of other defects, specific to amorphous SiO_2. Type II silicon-oxygen-deficiency center "SiODC(II)" is a much studied instance of such dangling bond/surface type defect. Its early assignment to "unrelaxed" oxygen vacancy has changed later to divalent Si atom, coordinated by 2 bridging oxygens in SiO_2 network on surface of silica or on inner surface of a structural void. (see [4,9,39] for review). After observation of "crystal-like" and "glass-like" NBOHCs in n-irradiated quartz [24] it is reasonable to expect similar findings for SiODC(II) too. Overlapping PL bands, similar to singlet PL of SiODC(II), with peaks between 4.2 and 4.4 eV have been reported in n-irradiated quartz [40]. However, the long-lived triplet PL band of SiODC(II) at 2.6…2.7 eV with lifetime τ of ≈10 ms has not been reported in quartz. Its decay constant can be regarded as the most unambiguous "fingerprint" of SiODC(II), since no other PL centers with τ in the 3.0.30 ms range are known in crystalline or glassy SiO_2. For example, a similarly positioned 2.7 eV PL band is reported in γ-irradiated quartz [5], however, its lifetime (3.6 ns) indicates its completely different origin.

The time-resolved "slow" PL band at 2.6 eV in n-irradiated quartz (Fig. 4a) has peak position, halfwidth and, the most important, the decay constant very close to those of SiODC(II) in glassy SiO_2 (Fig. 5): 2.6 vs. 2.7 eV, 0.38 vs. 0.4 eV and 8.7 vs. 9.9 ms, respectively. This confirms that SiODC(II) is created in n-irradiated quartz. This conclusion is further corroborated by the presence of the expected singlet PL band of SiODC(II) (Fig. 6), with peak position and fwhm (4.38 eV/0.35 eV @300 K) close to those in glass (4.3.0.4.4 eV/0.37 eV [4]).

Different from the case of NBOHCs, the low-temperature UV PL of SiODC(II) (Fig. 6) does not show any zero-phonon or vibronic sharp lines above the noise level. The expected ZPL position is at ≈4.7 eV, halfway between the peaks of PL (4.4 eV) and excitation (5.04 eV [4]). Arbitrary assuming "average" energy of the coupled phonons/local vibrations as $\hbar\omega \approx 600\,cm^{-1}$, the Huang-Rhys factor S can be estimated as (Stokes shift)/2ħω ≈ 4 and the expected intensity of ZPL relative to the entire spectrum as $e^{-S} \approx 0.02$. Sharp line of this magnitude should be detectable even on the relatively high noise background of Fig. 6. Its absence indicates that either the neutron-created SiODC(II) are all strongly inhomogeneously broadened (unlike the case of NBOHC's), or that actual S values are significantly larger than 4 due to interactions with lower energy phonons, and therefore the ZPL intensity is low even in the absence of inhomogeneous broadening.

In the case of e-irradiated quartz, the characteristic slow triplet PL of SiODC(II) is not found (Fig. 4b), despite the high detectivity of time-resolved/laser-excited PL technique. On the other hand, as discussed above, NBOHC's are created in the same sample (Figs. 1–4). This may indicate that a larger scale local damage, as compared to simple O vacancies or NBOHCs, is needed to create divalent Si in quartz. This conclusion is in accord with the observations that SiODC(II) is most efficiently created by types of irradiation, which cause a massive localized damage (amorphization, nanovoids): ion beam [41], fs-laser writing [42,43], and is not created by "soft" (e.g., γ- or electron) irradiation [5,6], capable of displacing only single oxygen atoms.

The closest crystal analog to the two-fold coordinated (divalent) Si atom in amorphous SiO_2 is oxygen divacancy, which can be viewed as divalent Si, neighbored by two Si dangling bonds, created by a removal of two bridging oxygen atoms from SiO_4 tetrahedron in α-quartz lattice. It has been suggested [44] as a "bulk" version of "surface-type", isolated divalent Si. This idea can be reviewed in the light of the present results.

The lower limit of the concentration of O divacancies in our α-quartz sample can be roughly estimated, by assuming that the oxygen atoms are displaced only by the knock-on damage, disregarding other efficient creation mechanisms, like ionization. Using oxygen displacement threshold energy 50 eV and electron beam energy 2.5 MeV, the oxygen knock-on cross section in SiO_2 can be calculated as $\sigma_K = 1.1 \times 10^{-23}\,cm^2$ (for details see the discussion on O displacement energy in SiO_2 and eq. 6 for evaluation of σ_K in review [26]). The probability of displacement of O atom by irradiation fluence $\Phi = 3 \times 10^{19}$ e^-/cm^2 is $W_1 = 1\text{-}\exp(-\Phi\sigma_K) \approx \Phi\sigma_K = 3.33 \times 10^{-4}$. With α-quartz having $N = 5.32 \times 10^{22}$ O atoms/cm^3, the estimated concentration of displaced O atoms, which roughly equals the concentration of O vacancies is $NW_1 = 1.77 \times 10^{19}\,cm^{-3}$.

To create O divacancy, one of the 6 oxygen atoms, neighboring the oxygen vacancy must be additionally displaced. Assuming unchanged O

displacement energy, the probability of this process is $W_2 = 6\,W_1^2 = 6.64 \times 10^{-7}$, and the estimated concentration of O divacancies is $NW_2 = 3.53 \times 10^{16}\,cm^{-3}$.

This concentration of divacancies should give an observable luminescence, if they were responsible for SiODC(II) PL: 10 times lower SiODC(II) concentrations are detectable in glassy SiO_2 by conventional PL spectrometers. The above estimates of vacancy and divacancy concentrations are very crude and can easily be wrong by 1–2 decimal orders of magnitudes, in particular, because they ignore the reverse process of vacancy-interstitial recombination. However, pulsed laser excitation and time-resolved multichannel recording technique gives an additional sensitivity increase margin of $> 10^3$ times and PL centers in concentrations $< 10^{14}\,cm^{-3}$ should be detectable. Therefore the data tentatively indicate that O divacancy in quartz crystal does not give PL bands similar to those of SiODC(II). Structural voids larger than represented by oxygen divacancy and a significant local damage, like in neutron tracks, could be necessary for SiODC(II) to form in quartz. This agrees well with the studies of Au^+ ion-beam damage in glassy SiO_2 [41], which indicate that SiODC(II) creation efficiency clearly correlates with nuclear energy loss.

4.3. Interstitial O_2

Infrared luminescence spectra of irradiated α-quartz show presence of $\approx 6 \times 10^{16}\,cm^{-3}$ interstitial O_2 molecules in n-irradiated sample (Fig. 7b) and their absence ($< 10^{15}\,cm^{-3}$, Fig. 7c,d) in e^- - irradiated samples. In the same time, the data discussed in the previous section indicate that at least $10^{18}\,cm^{-3}$ oxygen vacancies exist in the $10^{19}\,e^-/cm^3$ irradiated crystal. Different to the case of glassy SiO_2 [17], in the nearly intact crystal lattice of electron-irradiated α-quartz the displaced oxygen atom evidently does not dimerize to form interstitial O_2, but interacts instead with a normal "bridging"oxygen and forms a peroxy linkage (Si-O-O-Si bond), as predicted by most calculations, e.g., [45,46]. It is calculated that O_2 molecule in α-quartz can be located in the structural channels along the c-axis, forms an angle of 51° between O—O direction and c-axis, however, it is strongly confined and causes a distortion of the surrounding quartz lattice [47]. The estimated energy of incorporation of O_2 in interstitial voids increases from 0.5 to 3.5 eV when going from amorphous SiO_2 to α-quartz [48]. In contrast to these studies, interstitial O_2 was calculated to be the main diffusing species both in cristobalite and α-quartz structures [49]. However, the presence of interstitial O_2 in undamaged α-quartz has never been experimentally demonstrated, while there is ample Raman [19–21,23], PL[17,18,22,24], EPR [9] or diffusion-based evidence for O_2 in silica and silica-based glasses. The present data further confirm the results of the previous study [3], performed at ≈140× lower dose (0.051 GGy γ-rays), that the POL configuration rather than interstitial O_2 may be the preferable way of incorporation of excess oxygen in undamaged α-quartz lattice, and that creation of larger voids than available in an intact α-quartz structure is required for interstitial O_2 configuration to exist.

5. Conclusion

In this study, amorphous state-characteristic defects, oxygen dangling bonds (NBOHCs) were detected for the first time in *crystalline* SiO_2 irradiated by MeV electrons below the amorphization threshold. Compared to NBOHCs in amorphous SiO_2, they show significantly smaller inhomogeneous broadening and are thus well-suited for detailed spectroscopic studies. Further studies of their specific properties on crystalline and amorphous SiO_2 surfaces may be helpful in understanding the different toxicities of crystalline and amorphous SiO_2 surfaces, which are related to the high reactivity of surface NBOHCs [38,50]. In contrast, two other amorphous-state-characteristic defects, divalent Si atom ("SiODC(II)", silylene center) and interstitial O_2 molecule were *not* found in the same e^- −irradiated α-quartz samples. They were, however, present in neutron-irradiated quartz, evidently, in the particle tracks. The creation of divalent Si in neutron-irradiated quartz was unambiguously confirmed by detecting of its long-lived triplet luminescence. While divalent Si is less convenient than NBOHC for site-selective luminescence studies due to its stronger electron-phonon coupling, more detailed low T studies of divalent Si in quartz matrix look promising.

All three defects, NBOHC, divalent Si and O_2, require a presence of internal interstitial voids in SiO_2 with sizes, evidently larger than available in pristine α-quartz. However, only NBOHC's were found in e^- - irradiated quartz, exposed to doses below the amorphization threshold. It remains to establish whether they were created from their natural precursors, lattice-bound silanol groups (Si-O-H), typically decorating lattice defects in synthetic quartz, or that their appearance is the first mark of the onset of amorphization.

Acknowledgements

The support from M-ERANET project "MyND" is acknowledged. K.K. was partially supported by the Collaborative Research Project of Laboratory for Materials and Structures, Tokyo Institute of Technology. Visiting researcher support from Ecole Polytechnique, Palaiseau is appreciated. Mr. Olivier Cavani is thanked for the expert help with irradiations.

References

[1] W.H. Baur, In search of the crystal structure of low quartz, Z. Kristallogr. 224 (2009) 580–592.
[2] C.J. Benmore, E. Soignard, S.A. Amin, M. Guthrie, S.D. Shastri, P.L. Lee, J.L. Yarger, Structural and topological changes in silica glass at pressure, Phys. Rev. B 81 (2010) 054105 (1–5).
[3] K. Kajihara, L. Skuja, H. Hosono, Formation and annihilation of intrinsic defects induced by electronic excitation in high-purity crystalline SiO_2, J. Appl. Phys. 113 (2013) 143511(1–4).
[4] L. Skuja, The nature of optically active oxygen-deficiency-related centers in amorphous silicon dioxide, J. Non-Cryst. Solids 239 (1998) 16–48.
[5] M. Cannas, S. Agnello, F.M. Gelardi, R. Boscaino, A.N. Trukhin, P. Liblik, C. Lushchik, M.F. Kink, Y. Maksimov, R.A. Kink, Luminescence of γ-radiation-induced defects in α-quartz, J. Phys. Condens. Matter 16 (2004) 7931–7939.
[6] M. Cannas, S. Agnello, R. Boscaino, F.M. Gelardi, A. Trukhin, Photoluminescence in gamma irradiated alpha-quartz investigated by synchrotron radiation, Radiat. Meas. 38 (2004) 507–510.
[7] L. Skuja, K. Kajihara, M. Hirano, H. Hosono, Visible to vacuum-UV range optical absorption of oxygen dangling bonds in amorphous SiO_2, Phys. Rev. B 84 (2011) 205206(1–9).
[8] S. Girard, J. Kuhnhenn, A. Gusarov, B. Brichard, M. Van Uffelen, Y. Ouerdane, A. Boukenter, C. Marcandella, Radiation effects on silica-based optical fibers: recent advances and future challenges, IEEE Trans. Nucl. Sci. 60 (2013) 2015–2036.
[9] D.L. Griscom, Optical properties and structure of defects in silica glass, J. Ceram. Soc. Jpn. 99 (1991) 923–942.
[10] L. Skuja, The origin of the intrinsic 1.9 eV luminescence band in glassy SiO_2, J. Non-Cryst. Solids 179 (1994) 51–69.
[11] L. Vaccaro, M. Cannas, R. Boscaino, Luminescence features of nonbridging oxygen hole centres in silica probed by site-selective excitation with tunable laser, Solid State Commun. 146 (2008) 148–151.
[12] L. Vaccaro, M. Cannas, V. Radzig, Luminescence properties of nonbridging oxygen hole centers at the silica surface, J. Non-Cryst. Solids 355 (2009) 1020–1023.
[13] D.L. Griscom, Thermal bleaching of X-ray-induced defect centers in high-purity fused silica by diffusion of radiolytic molecular hydrogen, J. Non-Cryst. Solids 68 (1984) 301–325.
[14] L. Giordano, P.V. Sushko, G. Pacchioni, A.L. Shluger, Optical and EPR properties of point defects at a crystalline silica surface: Ab initio embedded-cluster calculations, Phys. Rev. B 75 (2007) 024109(1-9).
[15] K.-F. Klein, V.K. Khalilov, UV-fibers: two decades of improvement for new applications, Proc. SPIE 9317 (2015) 93170(S1-S14).
[16] M. Cannas, R. Boscaino, F.M. Gelardi, M. Leone, Stationary and time dependent PL emission of v-SiO_2 in the UV range, J. Non-Cryst. Solids 216 (1998) 99–104.
[17] K. Kajihara, M. Hirano, L. Skuja, H. Hosono, Intrinsic defect formation in amorphous SiO_2 by electronic excitation: bond dissociation versus Frenkel mechanisms, Phys. Rev. B 78 (2008) 094201(1-8).
[18] L. Skuja, B. Güttler, D. Schiel, A.R. Silin, Infrared photoluminescence of pre-existing or radiation-induced interstitial oxygen molecules in glassy SiO_2 and α-quartz, Phys. Rev. B 58 (1998) 14296–14304.
[19] N. Ollier, B. Champagnon, B. Boizot, Y. Guyot, G. Panczer, B. Padlyak, Influence of external beta-irradiation in oxide glasses, J. Non-Cryst. Solids 323 (2003) 200–206.
[20] N. Ollier, B. Boizot, B. Reynard, D. Ghaleb, G. Petite, Analysis of molecular oxygen formation in irradiated glasses: a Raman depth profile study, J. Nucl. Mater. 340 (2005) 209–213.

[21] A.H. Mir, M. Toulemonde, C. Jegou, S. Miro, Y. Serrys, S. Bouffard, S. Peuget, Understanding and simulating the material behavior during multi-particle irradiations, Sci. Rep. 6 (2016) 30191 (1 – 11).
[22] M.A. Stevens-Kalceff, Electron-irradiation-induced radiolytic oxygen generation and microsegregation in silicon dioxide polymorphs, Phys. Rev. Lett. 84 (2000) 3137–3140.
[23] M. Lancry, B. Poumellec, J. Canning, K. Cook, J.-C. Poulin, F. Brisset, Ultrafast nanoporous silica formation driven by femtosecond laser irradiation, Laser Photon. Rev. 7 (2013) 953–962.
[24] L. Skuja, K. Kajihara, M. Hirano, H. Hosono, Oxygen-excess-related point defects in glassy/amorphous SiO_2 and related materials, Nucl. Instrum. Meth. Phys. Res. B286 (2012) 159–168.
[25] H. Inui, H. Mori, T. Sakata, H. Fujita, Electron irradiation induced crystalline-to-amorphous transition in quartz single crystals, J. Non-Cryst. Solids 116 (1990) 1–15.
[26] N. Jiang, Electron beam damage in oxides: a review, Rep. Prog. Phys. 79 (2016) 016501(1-33).
[27] NIST Estar, Stopping Power and Range Tables for Electrons, https://physics.nist.gov/PhysRefData/Star/Text/ESTAR.html.
[28] J. Etchepare, M. Merian, L. Smetankine, Vibrational normal modes of SiO_2. I. α and β quartz, J. Chem. Phys. 60 (1974) 1873–1876.
[29] S.M. Shapiro, D.C. O'Shea, H.Z. Cummins, Raman scattering study of the alpha-beta phase transition in quartz, Phys. Rev. Lett. 19 (1967) 361–364.
[30] L. Skuja, K. Kajihara, J. Grube, H. Hosono, Luminescence of non-bridging oxygen hole centers in crystalline SiO_2, AIP Conf. Proc. 1624 (2014) 130–134.
[31] A.N. Streletsky, A.B. Pakovich, V.F. Gachkovsky, Yu. Aristov, Yu. Rufov, I. Butyagin, Luminescent properties of mechanical defects on surface of quartz, Khim. Fiz. (Sov. Chem. Phys.) 7 (1982) 938–946.
[32] L. Vaccaro, M. Cannas, The structural disorder of a silica network probed by site selective luminescence of the nonbridging oxygen hole centre, J. Phys. Condens. Matter 22 (2010) 235801(1–6).
[33] M. Zanatta, G. Baldi, R.S. Brusa, W. Egger, A. Fontana, E. Gilioli, S. Mariazzi, G. Monaco, L. Ravelli, F. Sacchetti, Structural evolution and medium range order in permanently densified vitreous SiO_2, Phys. Rev. Lett. 112 (2014) 045501(1-5).
[34] M. Hasegawa, M. Saneyasu, M. Tabata, Z. Tang, Y. Nagai, T. Chiba, Y. Ito, Positron and positronium studies of irradiation-induced defects and microvoids in vitreous metamict silica, Nucl. Instrum. Meth. Phys. Res. B166-B167 (2000) 431–439.
[35] R.S. Brusa, S. Mariazzi, L. Ravelli, P. Mazzoldi, G. Mattei, W. Egger, C. Hugenschmidt, B. Löwe, P. Pikart, C. Macchi, A. Somoza, Study of defects in implanted silica glass by depth profiling positron annihilation spectroscopy, Nucl. Instrum. Meth. Phys. Res. B268 (2010) 3186–3190.
[36] M.R. Pascucci, J.L. Hutchison, L.W. Hobbs, The metamict transformation in alpha-quartz, Radiat. Eff. 74 (1983) 219–226.
[37] L. Douillard, J.P. Duraud, Swift heavy ion amorphization of quartz — a comparative study of the particle amorphization mechanism of quartz, Nucl. Instrum. Meth. Phys. Res. B107 (1997) 212–217.
[38] F. Musso, P. Ugliengo, X. Solans-Monfort, M. Sodupe, Periodic DFT study of radical species on crystalline silica surfaces, J. Phys. Chem. C114 (2010) 16430–16438.
[39] L. Skuja, Isoelectronic series of twofold coordinated Si, Ge, and Sn atoms in glassy SiO_2: a luminescence study, J. Non-Cryst. Solids 149 (1992) 77–95.
[40] A. Corazza, B. Crivelli, M. Martini, G. Spinolo, A. Vedda, Photoluminescence and optical absorption in neutron-irradiated crystalline quartz, Phys. Rev. B 53 (1996) 9739–9744.
[41] Tengfei Yang, Yuan Gao, Xuejun Huang, Yanwen Zhang, Marcel Toulemonde, Jianming Xue, Sha Yan, Yugang Wang, The transformation balance between two types of structural defects in silica glass in ion-irradiation processes, J. Non-Cryst. Solids 357 (2011) 3245–3250.
[42] M. Beresna, M. Gecevičius, M. Lancry, B. Poumellec, P.G. Kazansky, Broadband anisotropy of femtosecond laser induced nanogratings in fused silica, Appl. Phys. Lett. 103 (2013) 131903(1-5).
[43] M. Watanabe, S. Juodkazis, H.-B. Sun, S. Matsuo, H. Misawa, Luminescence and defect formation by visible and near-infrared irradiation of vitreous silica, Phys. Rev. B 60 (1999) 9959–9964.
[44] D.L. Griscom, Trapped-electron centers in pure and doped glassy silica: a review and synthesis, J. Non-Cryst. Solids 357 (2011) 1945–1962.
[45] D. Ricci, G. Pacchioni, M.A. Szymanski, A.L. Shluger, A.M. Stoneham, Modeling disorder in amorphous silica with embedded clusters: the peroxy bridge defect center, Phys. Rev. B 64 (2001) 224104-(1-8).
[46] B. Winkler, L. Martin-Samos, N. Richard, L. Giacomazzi, A. Alessi, S. Girard, A. Boukenter, Y. Ouerdane, M. Valant, Correlations between structural and optical properties of peroxy bridges from first principles, J. Phys. Chem. C 121 (2017) 4002–4010.
[47] P.V. Sushko, A.L. Shluger, The effect of the α-quartz lattice on the optical absorption and stretching frequency of the interstitial O_2 molecule, Phys. Status Solidi 2C (2005) 503–506.
[48] A. Bongiorno, A. Pasquarello, Multiscale modeling of oxygen diffusion through the oxide during silicon oxidation, Phys. Rev. B 70 (2004) 195312(1-14).
[49] T. Hoshino, M. Hata, S. Neya, Y. Nishioka, T. Watanabe, K. Tatsumura, I. Ohdomari, Diffusion of molecular and atomic oxygen in silicon oxide, Jpn. J. Appl. Phys. 42 (2003) 3560–3565.
[50] A. Rimola, D. Costa, M. Sodupe, J.-F. Lambert, P. Ugliengo, Silica surface features and their role in the adsorption of biomolecules: computational modeling and experiments, Chem. Rev. 113 (2013) 4216–4313.